Materials Today Bio 24 (2024) 100927

Contents lists available at ScienceDirect

Materials Today Bio

journal homepage: www.journals.elsevier.com/materials-today-bio

Celecoxib and cisplatin dual-loaded microspheres synergistically enhance transarterial chemoembolization effect of hepatocellular carcinoma

Kunpeng Wu [a,b,c,1], Shengnan Ma [d,**,1], Xiaohong Xu [a,b,c], Yiming Liu [a,b,c], Chuan Tian [e], Chengzhi Zhang [a,b,c], Jiheng Shan [a,b,c], Zongming Li [a,b,c], Kewei Ren [a,b,c], Jianzhuang Ren [a,b,c,***], Xinwei Han [a,b,c,****], Yanan Zhao [a,b,c,*]

[a] Department of Interventional Radiology, Key Laboratory of Interventional Radiology of Henan Province, The First Affiliated Hospital of Zhengzhou University, Zhengzhou, 450052, China
[b] Interventional Institute of Zhengzhou University, Zhengzhou, 450052, China
[c] Interventional Treatment and Clinical Research Center of Henan Province, Zhengzhou, 450052, China
[d] Department of Endocrinology and Metabolism, The First Affiliated Hospital of Zhengzhou University, Zhengzhou University, Zhengzhou, 450052, Henan, China
[e] Department of Interventional Medical Center, the Affiliated Hospital of Qingdao University, No. 1677 Wutaishan Road, Shandong, 266000, Qingdao, China

ARTICLE INFO

Keywords:
Transarterial chemoembolization
Drug-eluting microspheres
Cisplatin
Celecoxib
Antitumor effect

ABSTRACT

Transarterial chemoembolization (TACE) is a first-line treatment for intermediate to advanced-stage liver cancer, with drug-eluting microspheres commonly used as embolic agents. However, currently available drug-eluting microspheres suffer from low drug-loading capacity and limited drug options. In this work, we developed polydopamine-modified polyvinyl alcohol dual-drug-loaded microspheres encapsulating celecoxib and cisplatin (referred to as PCDMS). Physicochemical characterization revealed that the surface of the microspheres displayed increased roughness after polydopamine modification, and celecoxib and cisplatin were successfully loaded onto the microsphere surface. In vitro cell experiments demonstrated that the PCDMS significantly inhibited the proliferation and migration of highly metastatic human liver cancer cells (MHCC-97H) and human liver cancer cells (SMMC-7721). Furthermore, the dual-loaded microspheres exhibited remarkable tumor growth inhibition and reshaped the tumor microenvironment in both subcutaneous H22 liver cancer model in Balb/c mice and intrahepatic VX2 tumor model in New Zealand rabbits, demonstrating a synergistic antitumor effect where $1 + 1 > 2$. This work provides a potential therapeutic approach for the treatment of refractory liver cancer and holds significant translational potential.

1. Introduction

Hepatocellular carcinoma (HCC) is the most common type of liver cancer, accounting for approximately 90 % of primary liver malignancies [1]. Current therapeutic approaches for HCC encompass surgical resection, liver transplantation, image-guided percutaneous ablation, radiation therapy, transarterial chemoembolization (TACE), and systemic pharmacotherapy (including chemotherapy, targeted therapy, and immunotherapy) [2]. Among these, TACE has gained global acceptance as the standard treatment modality for intermediate-stage HCC due to its high efficacy, minimal invasiveness, and strong repeatability [3].

* Corresponding author. Department of Interventional Radiology, Key Laboratory of Interventional Radiology of Henan Province, The First Affiliated Hospital of Zhengzhou University, Zhengzhou, 450052, China.
** Corresponding author. Department of Endocrinology and Metabolism, The First Affiliated Hospital of Zhengzhou University, Zhengzhou University, Zhengzhou, 450052, Henan, China.
*** Corresponding author. Department of Interventional Radiology, Key Laboratory of Interventional Radiology of Henan Province, The First Affiliated Hospital of Zhengzhou University, Zhengzhou, 450052, China.
**** Corresponding author. Department of Interventional Radiology, Key Laboratory of Interventional Radiology of Henan Province, The First Affiliated Hospital of Zhengzhou University, Zhengzhou, 450052, China.
E-mail addresses: mashengnan@zzu.edu.cn (S. Ma), rjzjrk@126.com (J. Ren), fcchanxw@zzu.edu.cn (X. Han), yananzhao996@163.com (Y. Zhao).
[1] Kunpeng Wu and Shengnan Ma contributed equally to this work.

https://doi.org/10.1016/j.mtbio.2023.100927
Received 25 September 2023; Received in revised form 10 December 2023; Accepted 18 December 2023
Available online 28 December 2023

Compared to iodized oil and gelatin sponges, drug-loaded microspheres have advantages such as slow release, prolonged embolization, and low recanalization rate, making them one of the most commonly used TACE embolic agents [4]. The drug-loaded microspheres currently used in clinical practice include Callispheres®, DC Bead®, and Hepasphere®. These microspheres, usually made of polyvinyl alcohol (PVA), are used to adsorb and load drugs through positive-negative ion exchange [5]. However, this technology limits the amount of drug loading and is susceptible to mutual interference in the case of multiple drug loading, which greatly reduces the drug loading rate [6]. Dopamine (DA), a neurotransmitter, can undergo self-polymerization under certain conditions to form polydopamine (PDA). The PDA shell can wrap around the surface of almost all solid materials, and its consistency with abundant catechol structures exhibits strong adhesion [7]. In addition, studies confirmed that PDA has good biocompatibility and biodegradability, with good safety [8]. Thus, the adhesion of PDA can not only solve the problem of low drug loading rate but also realize the purpose of double drug loading.

Currently, commonly used chemotherapeutic agents in TACE for the treatment of HCC include doxorubicin, cisplatin (DDP), irinotecan, 5-fluorouracil, arsenic trioxide, and oxaliplatin [9]. DDP, a first-generation platinum-based chemotherapeutic agent, possesses a broad spectrum of anticancer activity, unique mechanisms of action, compatibility with combination therapy, and affordability [10]. Nevertheless, DDP suffers from poor water solubility, limited bioavailability, nephrotoxicity, neurotoxicity, severe gastrointestinal reactions, bone marrow suppression, and susceptibility to drug resistance, all of which restrict its clinical utility [11]. Hence, there is an urgent need to explore measures to mitigate DDP resistance, diminish adverse effects, and concurrently enhance synergistic effects to render liver cancer cells more responsive to the medication.

Celecoxib (CXB), as a selective COX-2 inhibitor and nonsteroidal

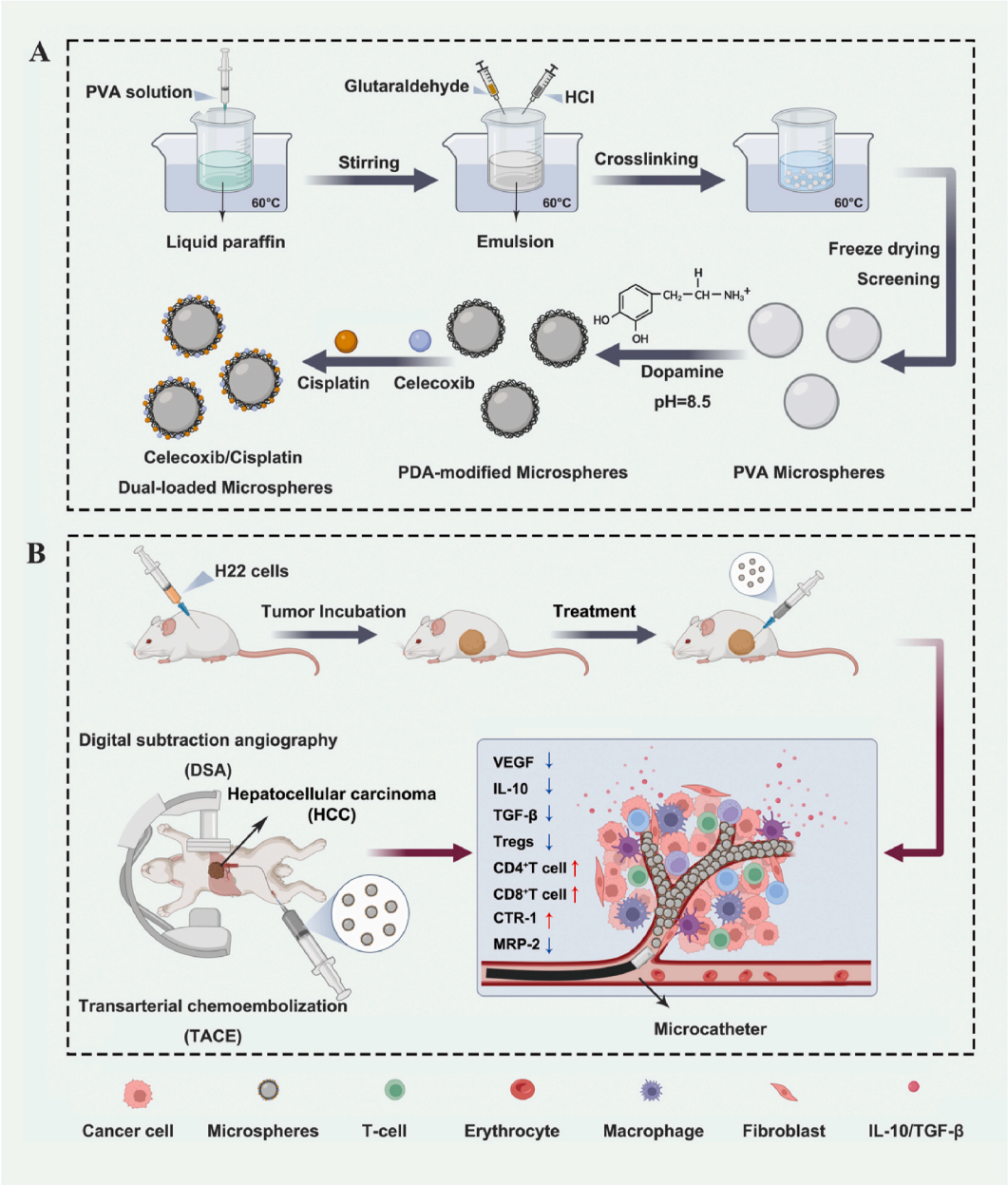

Scheme 1. Celecoxib/Cisplatin dual-loaded microspheres (PCDMS) synergistically enhance the transarterial chemoembolization effect of hepatocellular carcinoma (Created in Biorender.com). **(A)** Construction process of PCDMS. **(B)** PCDMS was used on a mouse xenograft tumor model; PCDMS was used for hepatocellular carcinoma embolism in a rabbit VX2-tumor bearing model.

anti-inflammatory drug, is widely used to treat pain and inflammation [12]. It can reduce the expression level of COX-2 in tumor tissues, thereby reducing the secretion of MMP-2 (Matrix metalloproteinases-2) and MMP-9 (Matrix metalloproteinases-9), inhibiting tumor angiogenesis, weakening tumor invasion and metastasis, and providing a better tumor microenvironment for the action of chemotherapy drugs [13]. Importantly, CXB down-regulates the expression of multi-drug resistance proteins (MRP-2 and MRP-4) and up-regulates the expression of copper transporter 1 (cr-1) in liver cancer cells, thereby promoting the accumulation of cisplatin in cells, reducing the resistance of tumor cells to cisplatin, and enhancing cytotoxicity [14]. Moreover, CXB can reduce the recruitment of tumor-associated macrophages and reduce the activity of regulatory T cells (Tregs), thereby reducing immunosuppression, increasing the infiltration of CD4 and CD8 cytotoxic T lymphocytes, enhancing immune cytotoxicity, and further enhancing the toxic effect of DDP [15].

Therefore, this study aims to use PDA-modified PVA microspheres to dual-load DDP and CXB (Scheme 1A), achieving high drug-loading capacity and enhanced synergistic transarterial chemoembolization effect of HCC on a mouse xenograft tumor model and a rabbit VX2-tumor bearing model (Scheme 1B). The dual-loaded microspheres can overcome the resistance of liver cancer cells to DDP, reshape the local tumor microenvironment, and effectively suppress tumor growth and recurrence, achieving a synergistic anti-tumor effect where $1 + 1 > 2$.

2. Materials and methods

2.1. Materials

Polyvinyl alcohol (PVA) was obtained from Shanghai Macklin Biochemical Technology Co., Ltd. Celecoxib and cisplatin were provided by Sigma-Aldrich Trading Co., Ltd. Metastatic human liver cancer cells (MHCC-97H) and human liver cancer cells (SMMC-7721) were obtained from the Shanghai Cell Center (Chinese Academy of Sciences). Dulbecco's modified Eagle's medium, fetal bovine serum, penicillin-streptomycin, and trypsin-EDTAwere supplied by Sigma-Aldrich Trading Co., Ltd. The Cell Counting Kit-8 (CCK-8) and cell cycle detection kits were purchased from Abbkine Scientific Co., Ltd. The live/dead viability kits were sourced from Thermo Fisher Scientific Co., Ltd. Other chemical and reagents were used without modification.

2.2. Preparation of dual-loaded microspheres

Uniform-sized microspheres of polyvinyl alcohol (PVA) were prepared using the emulsion crosslinking technique [16]. A 0.2 % dopamine solution was prepared using Tris-HCl buffer as the solvent. Subsequently, the microspheres were immersed in the dopamine solution, and the pH was adjusted to 8.5. The reaction was carried out under mechanical stirring at room temperature. After 48 h, the microspheres were washed with deionized water to remove unreacted dopamine and then centrifuged to obtain polydopamine-modified PVA microspheres (named PMS).

A solution of 50 mg of celecoxib powder in 10 mL of PBS buffer was prepared and mixed thoroughly to obtain a celecoxib solution. Similarly, an explanation of 20 mg of cisplatin powder in 10 mL of PBS buffer was prepared and mixed well to get a cisplatin solution. A mixture of 20 mg of cisplatin powder and 50 mg of celecoxib powder was dissolved in 10 mL of PBS buffer and mixed thoroughly to obtain a celecoxib/cisplatin co-mixture solution. Subsequently, 100 mg of polydopamine-modified PVA microspheres were added separately to the three solutions mentioned above and incubated on a shaker for 24 h, followed by centrifugation at 3000 rpm for 10 min. This process yielded celecoxib microspheres (named PCMS), cisplatin microspheres (named PDMS), and celecoxib/cisplatin microspheres (named PCDMS).

2.3. Physicochemical characterization of dual-loaded microspheres

The SEM images and EDS spectra of the test samples were obtained using a JSM-7401F microscope equipped with an energy-dispersive spectroscopy (EDS) system, allowing analysis of the surface morphology and elemental composition of the samples [17]. Fourier-transform infrared spectroscopy (FTIR) was performed on the samples using a TNZ1-5700 spectrometer (Nicolet, USA), with a scanning range of 500–4000 cm^{-1}. The properties and chemical states of the pieces were analyzed using an X-ray photoelectron spectrometer, with a measurement range of 1200-0 cm $^{-1}$.

2.4. Drug loading and release characteristics of dual-loaded microspheres

2.4.1. Drug loading behavior of dual-loaded microspheres

20 mg of celecoxib and 10 mg of cisplatin were separately transferred to 10 mL volumetric flasks. Physiological saline solution was added to make up the volume, and the solutions were thoroughly mixed, resulting in a concentration of 2 mg/mL for celecoxib and 1 mg/mL for cisplatin. Aliquots of 0.02, 0.05, 0.1, 0.5, 1.0, and 5.0 mL of each solution were taken and sequentially diluted with 10 mL volumetric flasks to obtain solutions with concentrations of 2, 5, 10, 20, 100, and 500 μg/mL. The absorbance of each solution was measured using a UV spectrophotometer, and a standard curve was constructed [18].

The test samples were thoroughly vortexed and then allowed to stand for 24 h. After that, they were centrifuged at 12,000 rpm for 10 min. The supernatant (160 μL) was collected, and the absorbance was measured using a UV spectrophotometer to determine the content of celecoxib and cisplatin in the supernatant (W1). The encapsulation efficiency (ER) was then calculated as follows:

$$\mathrm{ER}\ (\%) = [(\mathrm{W} - \mathrm{W1}) \ / \ \mathrm{W}] \times 100\%,$$

where W represents the initial drug loading amount (mg).

2.4.2. Drug release behavior of dual-loaded microspheres

The drug-loaded microspheres, with the supernatant removed, were placed in 15 mL clean centrifuge tubes for drug release. The release medium was deionized water with a pH of 7.4. The temperature of the thermostatic shaker was set at 37 °C, with a rotation speed of 100 rpm. Samples were collected at 6 h, 12 h, 1 day, 2 days, 3 days, 4 days, 5 days, 6 days, 7 days, 8 days, 10 days, 12 days, and 14 days. After each sampling, an equal volume of blank release medium (physiological saline solution) was immediately replenished. The absorbance of each sample was measured, and the cumulative drug release percentage was calculated for each group of drug-loaded microspheres.

2.5. Inhibitory effect of dual-loaded microspheres on MHCC-97H and SMMC-7721 cells

To evaluate the *in vitro* cytotoxicity of the dual drug-loaded microspheres, the highly metastatic liver cancer cells (MHCC-97H) and liver cancer cells (SMMC-7721) were selected as seed cells. Each group of samples was soaked in PBS for 24 h, and after centrifugation, the supernatant was collected as the extract for further use. This study was divided into seven groups: (1) NC (PBS as negative control), (2) PVA, (3) PMS, (4) PCMS, (5) PDMS, (6) PCDMS, and (7) PC (free CXB + DDP as a positive control).

2.5.1. CCK-8 assay

The digested cells were seeded in a 96-well plate (100 μL/well) and placed in a 37 °C, 5 % CO_2 incubator. After the cells were adhered entirely, they were washed three times with PBS and treated with the extract from each group. After incubating for 24, 48, and 72 h, 10 μL of CCK-8 reagent was added to each well, and the cells were further incubated for 3 h for color development. The optical density (OD) was

measured at 450 nm using an enzyme-linked immunosorbent assay (ELISA) reader.

2.5.2. Live/dead cell staining

The digested cells were seeded in a 24-well plate and placed in a 37 °C, 5 % CO_2 incubator. After the cells were adhered entirely, they were washed three times with PBS and treated with the extract from each group. A cell staining solution was prepared by diluting 5 μL of 4 mM Calcein-AM (Component A) and 20 μL of 1 mM ethidium homodimer-1 (Component B) in 10 mL of PBS. After 24 h of incubation, 500 μL of the cell staining solution was added to each group, and the plate was incubated in the dark at room temperature for 20 min. The cells were then transferred to an inverted fluorescence microscope for imaging.

2.5.3. Cell cycle analysis

The digested cells were seeded in a 35 mm culture dish and placed in a 37 °C, 5 % CO_2 incubator. The cells were then treated with the extract and incubated for an additional 24 h. The cells were collected in a 15 mL centrifuge tube using trypsin without EDTA, centrifuged at 1000 rpm for 5 min, and washed twice with pre-chilled PBS. The cell density was adjusted to (2–4) × 10^6 cells/mL and resuspended in an EP tube. The supernatant was removed, and 500 μL of Binding Buffer was added. Each EP tube was supplemented with 5 μL of Annexin FITC and 5 μL of PI for cell resuspension. The tubes were incubated at room temperature in the dark for 15 min, and flow cytometry was used for analysis.

2.5.4. Scratch assay

The digested cells were seeded in a 24-well plate and placed in a 37 °C, 5 % CO_2 incubator. After overnight incubation, when the cell fusion reached over 90 %, a straight line was drawn in the center area of cell growth at the bottom of the culture dish using a 200 μL sterile pipette tip. The scratched cells were removed by washing three times with PBS, and fresh culture medium and the extract from each group were added. After 48 h of incubation, photographs were taken.

2.5.5. Transwell experiment

After treating the cells with various extract solutions, the digested and suspended cells were placed in a serum-free medium. Using a cell counter, the percentage of viable cells was recorded, and the cell density was adjusted based on the rate of viable cells, aiming for a density of 2 × 10^5 cells/ml. Then, 200 μL of the cell suspension was seeded onto the upper chamber of a Transwell with an 8 μm pore size. In the lower chamber, 600 μL of culture medium containing 20 % fetal bovine serum was added. The cells were cultured for 24 h. After removing the medium from the upper chamber, a cotton swab was used to wipe off the cells that did not migrate through the upper chamber. The cells were washed thrice with PBS and fixed with 4 % paraformaldehyde for 20 min. After the fixative was removed, the cells were washed three times with PBS. Subsequently, the cells were stained with 0.1 % crystal violet for 20 min, followed by another three washes with PBS. Finally, ten random fields of view were selected under a microscope for photography and cell counting.

2.6. In-vivo animal experiment of dual-loaded microspheres on subcutaneous H22 transplanted tumors in mice

2.6.1. Construction of the balb/c mouse subcutaneous H22 transplanted tumor model

Twenty-five 5-week-old female BALB/c mice were randomly divided into five groups: PVA treatment group, PMS treatment group, PCMS treatment group, PDMS treatment group, and PCDMS treatment group. The right axilla of each mouse was prepared and disinfected. Subsequently, 1 × 10^8 cell suspension was injected subcutaneously into the axilla of each mouse. Tumor growth was observed daily, and when the tumor volume reached 100 mm^3, each mouse was intratumorally injected with 100 mg of the sample for treatment. The body weight and tumor volume were measured every two days. This study was divided into six groups: (1) PVA, (2) PMS, (3) PCMS, (4) PDMS, (5) PCDMS, and (6) PC (free CXB + DDP as a positive control).

2.6.2. Biochemical analysis and sample collection

After euthanizing the mice, surgical dissection was performed to examine the tumors. Following the skin incision, the tumors were carefully separated from the surrounding muscular tissue in layers and photographed for assessment. A portion of the tumor was used for HE staining, IL-6 staining, TNF-α staining, Ki67 staining, VEGF staining, CD31 staining, IL-10 staining, and TGF-β staining. Another portion of the tumor was digested into single cells for CD3/CD4 and CD3/CD8 flow cytometry analysis. Additionally, samples of the heart, liver, spleen, lungs, and kidneys were obtained simultaneously for HE staining.

2.7. In vivo animal experiment of dual-loaded microspheres inhibiting VX2 liver transplanted tumors in rabbits

2.7.1. Construction of rabbit VX2 liver transplanted tumor model

The VX2 tumor tissue was cut into approximately 1 mm^3 pieces and suspended in 0.5 mL of physiological saline. The suspension was then inoculated into the lateral thigh muscle of the experimental rabbits. Two weeks after tumor implantation, palpable elastic masses with a diameter of 2–3 cm could be felt on the lateral thigh of the rabbits, indicating successful tumor establishment.

Before tumor implantation, the rabbits were fasted for 8 h. They were then anesthetized by intramuscular injection of 0.2 mg/kg of xylazine hydrochloride followed by 5 mg/kg of pentobarbital sodium. After the anesthesia took effect, the VX2 tumor tissue located in the lateral thigh muscle was exposed and dissected. The excised VX2 tumor tissue was placed in a sterile culture dish. Surrounding muscle tissue, blood vessels, fascia, and necrotic tissue were carefully removed, and the tumor tissue was washed three times with physiological saline. The viable VX2 tumor tissue was selected, minced, and stored for later use with a 21-gauge puncture needle.

The experimental rabbits were then placed in a supine position and fixed on a rabbit table after anesthesia. The surgical site was strictly sterilized using aseptic techniques. A 2–3 cm longitudinal incision was made along the midline of the abdomen, and the abdominal wall was dissected layer by layer to expose the liver. The left lobe of the liver was pulled out using hemostatic forceps, and a puncture needle was inserted into the liver parenchyma to a depth of 1 cm. After inserting the stylet, the puncture needle was withdrawn, and the puncture site was sealed with a gelatin sponge. The left lobe of the liver was gently pushed back into the abdomen, and the muscle and skin incisions were closed layer by layer. The wound was then disinfected.

To prevent infection, the rabbits were given intramuscular injections of cefotaxime sodium (0.1 mL/kg) for three consecutive days after surgery.

2.7.2. Transarterial chemoembolization (TACE)

After 2 weeks of intrahepatic implantation in rabbits, the growth of VX2 tumor tissue was evaluated using contrast-enhanced CT angiography to determine if it met the criteria for tumor formation, including the location and size of the VX2 tumor within the liver (Supplementary Material Fig.S1A). The rabbits were anesthetized as described earlier, and a venous indwelling needle (22G) was inserted into the marginal ear vein for administration. Siemens dual-source spiral CT scanning was employed. Once the tumor met the specified criteria, the rabbit's groin area on the right side was prepared and sterilized, and a vertical incision of 2 cm was made along the direction of the artery. The femoral artery in rabbits is relatively slender with thin walls and is often accompanied by the femoral vein and sciatic nerve within the fascia. A blunt glass cannula was used to gently separate the femoral artery, avoiding damage to the vein and nerve. The distal end of the right femoral artery was

temporarily occluded, and a no. 5 suture was used to elevate the proximal end of the artery (Supplementary Material Fig.S1B). With ophthalmic scissors, a small oblique incision was made towards the proximal end, and a 5-French sheath was inserted and secured. Under digital subtraction angiography (DSA), a 5-French catheter was introduced and advanced through the abdominal aorta to the level of the twelfth thoracic and first lumbar vertebrae to identify the opening of the celiac trunk. Subsequently, a 2.7-French microcatheter and a 0.021-inch guidewire were introduced, with the guidewire leading the way for catheter advancement. After entering the abdominal aorta, angiography was performed to determine the location and course of the hepatic artery. In rabbits, the abdominal aorta typically divides into three branches, with the centrally oblique branch being the hepatic artery. Once in the hepatic artery, superselective catheterization was performed to reach the tumor-feeding arteries, and the tumor was embolized according to the assigned treatment groups. After the treatment, angiography was performed again to confirm complete embolization of the tumor-feeding arteries. The microcatheter, guidewire, and guiding catheter were then removed, and the femoral artery was ligated. The muscle and skin incisions were closed in layers, and the sutured wounds were disinfected. All experimental rabbits received intramuscular injections of cefotaxime sodium (0.1 mL/kg) for 3 consecutive days to prevent infection.

2.7.3. Biochemical analysis

Blood samples were collected from the experimental rabbits at different time points: 7 days before TACE, and 1, 3, 7, and 14 days after TACE. Hematological parameters such as red blood cells, white blood cells, and platelets, as well as liver and kidney function markers including aspartate aminotransferase (AST), alanine aminotransferase (ALT), albumin (ALB), total bilirubin (TBIL), blood urea nitrogen (BUN), and serum creatinine (Cr) were analyzed.

2.7.4. Histological staining

After complete the removal of the rabbit liver, HE staining was performed to observe the embolization status. Tumor tissue samples from each group were fixed in formalin and used for HE staining, PCNA staining, CTR-1 staining, MRP-2 staining, CD4 staining, CD8 staining, and Foxp3 staining. Additionally, samples from the heart, spleen, lungs, and kidneys were also obtained for HE staining.

2.8. Statistical analysis

The results were expressed as the mean ± SD. Statistical analysis was performed using one-way ANOVA. Statistically significant values were indicated as * $P < 0.05$, ** $P < 0.01$, and *** $P < 0.001$.

3. Results

3.1. Evaluation of physicochemical property

The SEM results showed (Fig. 1A) that PVA particles exhibited a uniform spherical shape with a smooth and intact surface. PMS particles appeared elliptical or spheroidal in shape, with a rough surface characterized by wrinkles and unevenness. The morphologies of PCMS, PDMS, and PCDMS were similar to PMS, with the presence of drug crystals on their surfaces. Particle size analysis (Fig. 1B) indicated that PVA particles were concentrated around 100 μm, while PMS, PCMS, PDMS, and PCDMS exhibited increasing diameters, predominantly around 120 μm. Among them, PCDMS showed the highest increase in diameter. This increase can be attributed to the surface modification with PDA and the adsorption of drugs.

Furthermore, EDS elemental mapping was performed to analyze PCDMS. As shown in Fig. 1C, different elements (C, N, O, Pt, Cl, S, and F) were labeled with different colors on the surface of PCDMS samples. C and O were the main elements of PVA, while C, N, and O were the main elements of PDA. Pt and Cl were the main elements of DDP, and S and F were the main elements of CXB. The EDS results showed that C, N, O, Pt, Cl, S and F were evenly distributed on the surface of PCDMS, which confirmed that PDA successfully encapsulated PVA and loaded CXB and DDP.

Through the implementation of Fourier-transform infrared spectroscopy (FTIR) (Fig. 1D–E) and X-ray photoelectron spectroscopy (XPS) (Fig. 1F–G), the surface modification of PVA and the loading of drugs were verified. The results revealed distinctive peaks for PDA, ranging from 3215 to 3265 cm^{-1} and 1232 to 1493 cm^{-1}, and for CXB, ranging from 3232 to 3337 cm^{-1} and 1163 to 1348 cm^{-1}. Furthermore, specific peaks for DDP were observed, spanning from 3203 to 3248 cm^{-1}, 1299 to 1540 cm^{-1}, and 798 cm^{-1}, corresponding to the stretching vibrations of N–H. The presence of PDA peaks in PMS indicated the successful surface modification of the original PVA particles with PDA. Similarly, PCMS exhibited both PDA and CXB peaks, while PDMS displayed PDA and DDP peaks. Notably, PCDMS demonstrated prominent peaks of PDA, CXB, and DDP, indicating the encapsulation of both CXB and DDP within the PDA-modified microspheres. Likewise, the co-loading of CXB and DDP onto the surface of PMS was also confirmed through XPS analysis.

The loading and release of drugs serve as crucial indicators for evaluating the performance of drug-loaded microspheres. The encapsulation efficiency results (Fig. 1H) demonstrated that when PMS was solely loaded with drugs, the encapsulation rates for CXB and DDP were 70.79 ± 2.48 % and 74.97 ± 1.18 %, respectively. Meanwhile, when PMS was loaded with both CXB and DDP, the encapsulation rates were slightly reduced to 58.31 ± 2.45 % and 62.47 ± 2.96 %, respectively. The aforementioned outcomes revealed a slight impact on drug-loading efficiency when both drugs were co-loaded, yet the encapsulation rates remained above 50 %, ensuring a sustained high level of drug-loading efficiency.

Based on the cumulative drug release profiles (Fig. 1I–J), on the 14th day, the cumulative release rate of CXB was 92.54 ± 2.6 % for PCMS and 88.1 ± 1.38 % for PCDMS. Similarly, for DDP, the cumulative release rate was 88.69 ± 2.59 % for PDMS and 84.4 ± 2.56 % for PCDMS. These results indicate that PCMS, PDMS, and PCDMS exhibit stable *in vitro* drug release, enabling prolonged and controlled release, thereby meeting the pharmacological requirements for clinical therapy.

3.2. Inhibitory effects of PCDMS on liver cancer cells

To elucidate the effects of PCDMS on liver cancer cells, CCK-8, live/dead cell staining, apoptosis analysis, scratch assay and Transwell assay were used to study the effects of different groups of embolized microspheres extracts on the proliferation, apoptosis and migration of highly metastatic human liver cancer cells (MHCC-97H) and human liver cancer cells (SMMC-7721).

The CCK-8 results showed that CXB alone had limited inhibitory effects on tumor cells in both MHCC-97H (Fig. 2A) and SMMC-7721 (Fig. 3A). As time prolonged and drug concentration decreased, the inhibitory effect on cell proliferation further weakened. However, DDP alone and the combination therapy exhibited better abilities to inhibit tumor cell proliferation, showing a typical time-dependent pattern. As the duration of drug action increased, the proliferation ability of cells gradually diminished. Notably, inhibition in the PCDMS group was similar to that in the PC group and significantly higher than in the other groups.

Next, the effect of PCDMS on the migration and invasion ability of liver cancer cells was evaluated by scratch assay and Transwell assay. The results of the scratch assay (Fig. 2B–C; Fig. 3B–C) showed no significant difference in healing rate between the NC group and the PVA and PMS groups. The PCMS group exhibited a slightly slower healing rate compared to the NC group, while the PDMS and PCDMS groups showed a significantly reduced healing rate, particularly the PCDMS group. In addition, the healing rate of the PCDMS group was close to that

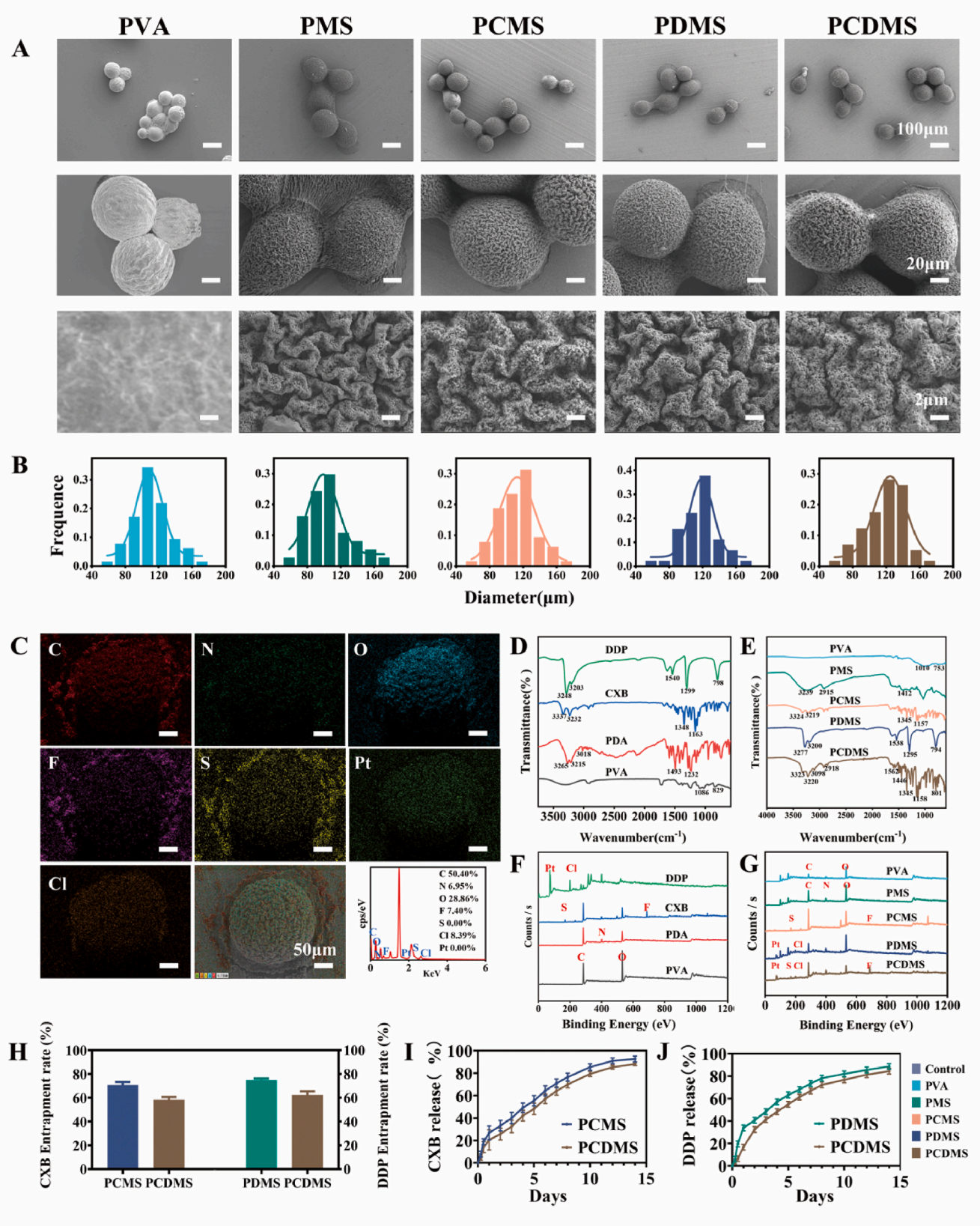

Fig. 1. Physicochemical characteristic. **(A)** Scanning electron microscopy (SEM) images at different magnifications, scale bars: 100 μm, 20 μm, and 2 μm. **(B)** Particle size analysis. **(C)** Elemental composition, scale bar: 50 μm. **(D)** FT-IR spectra of PVA, PDA, CXB, and DDP. **(E)** FT-IR spectra of microspheres in different groups. **(F)** XPS spectra of PVA, PDA, CXB, and DDP. **(G)** XPS spectra of microspheres in different groups. **(H)** Encapsulation rates of PCMS, PDMS, and PCDMS. **(I)** Drug release profiles of PCMS and PCDMS. **(J)** Drug release profiles of PDMS and PCDMS.

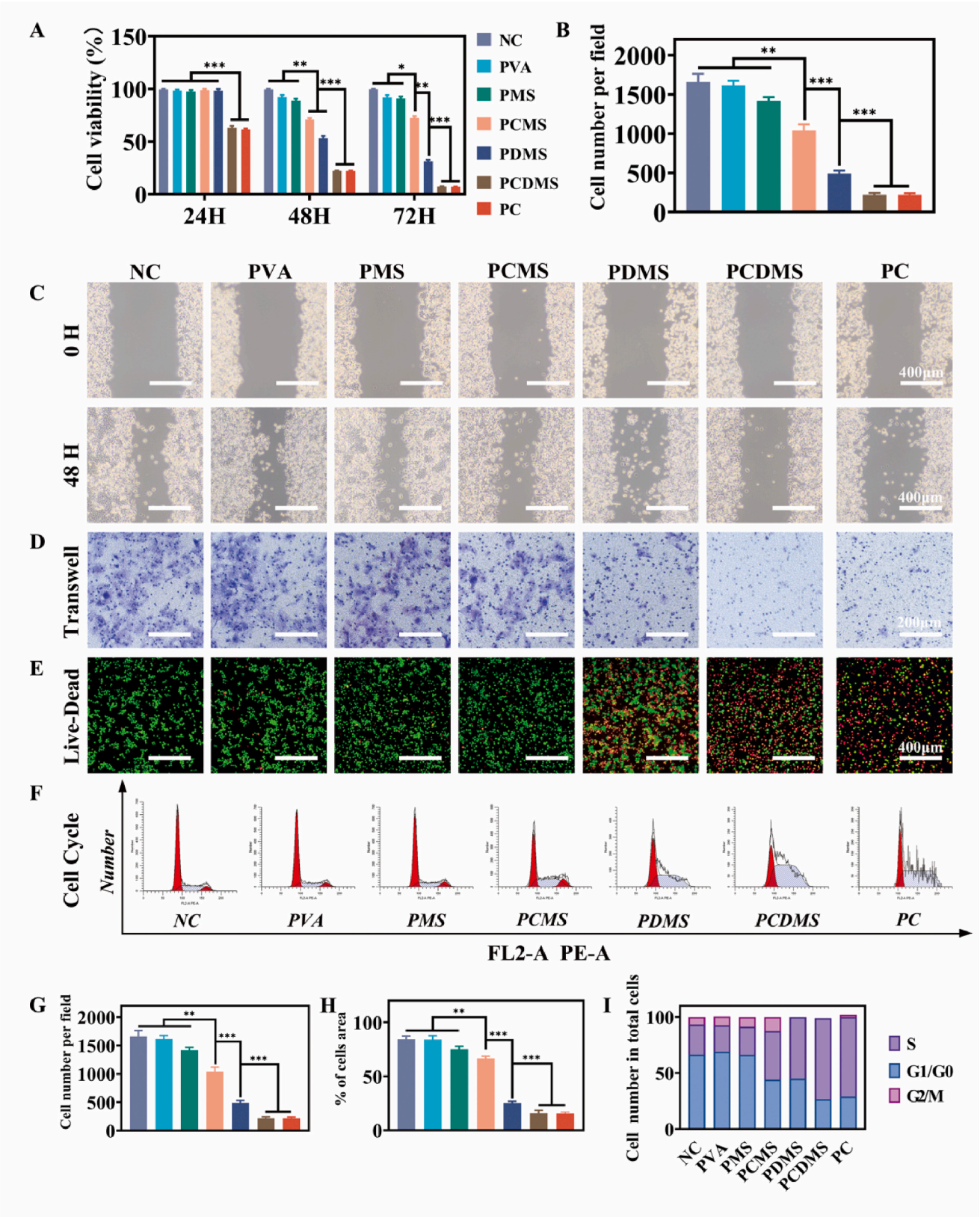

Fig. 2. The effects of PCDMS on MHCC-97H cells. **(A)** Cell viability assay. **(B)** Scratch assay migration distance percentage. **(C)** Scratch assay, scale: 400 μm. **(D)** Transwell assay, scale: 200 μm. **(E)** Live/dead cell staining, scale: 400 μm. **(F)** Cell cycle analysis. **(G)** Transwell assay cell count in the migration area. **(H)** Live/dead cell staining assay percentage of live cells. **(I)** Cell cycle analysis proportions of G1/G0, S, and G2/M phases. Significant differences: *P < 0.05, **P < 0.01, and ***P < 0.001.

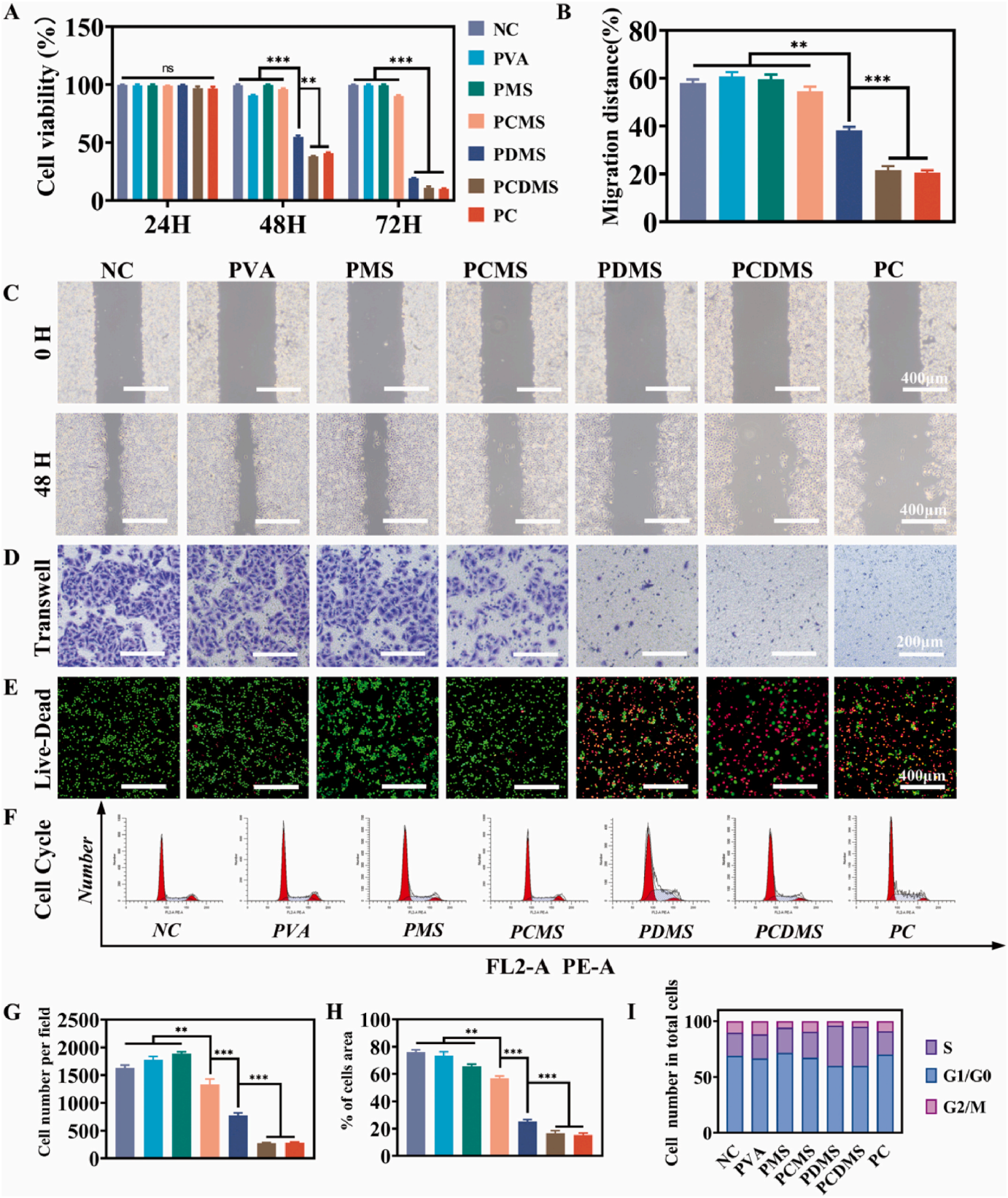

Fig. 3. The effects of PCDMS on SMMC-7721 cells. **(A)** Cell viability assay. **(B)** Scratch assay migration distance percentage. **(C)** Scratch assay, scale: 400 μm. **(D)** Transwell assay, scale: 200 μm. **(E)** Live/dead cell staining, scale: 400 μm. **(F)** Cell cycle analysis. **(G)** Transwell assay cell count in the migration area. **(H)** Live/dead cell staining assay percentage of live cells. **(I)** Cell cycle analysis proportions of G1/G0, S, and G2/M phases. Significant differences: *P < 0.05, **P < 0.01, and ***P < 0.001.

of the PC group. Similarly, the Transwell assay results (Fig. 2D,G; Fig. 3D,G) indicated that the PVA and PMS groups had no significant impact on the invasion and migration abilities of liver cancer cells compared to the NC group. Both PCMS and PDMS groups inhibited the invasion and migration of liver cancer cells, while PCDMS group significantly inhibited the migration and invasion of MHCC-97H and SMMC-7721 cells, similar to PC group. These findings suggest that CXB and DDP individually loaded into microspheres have certain inhibitory effects on both types of liver cancer cells. However, PCDMS, which simultaneously loads both drugs, synergistically inhibits the proliferation, migration, and invasion abilities of liver cancer cells.

The results of live/dead fluorescence staining of cells incubated with extract from different groups for 24 h showed the following in MHCC-97H cells (Fig. 2E,H): the percentage of live cells in the NC, PVA, PMS, PCMS, PDMS, PCDMS and PC groups was 84.39 % ± 2.93 %, 84.15 % ± 3.39 %, 75.15 % ± 2.53 %, 66.53 % ± 2.22 %, 25.25 % ± 1.53 %, 15.99 % ± 2.49 % and 15.76 % ± 1.06 %, respectively. Similar trends were observed in SMMC-7721 cells (Fig. 3E,H). The percentage of

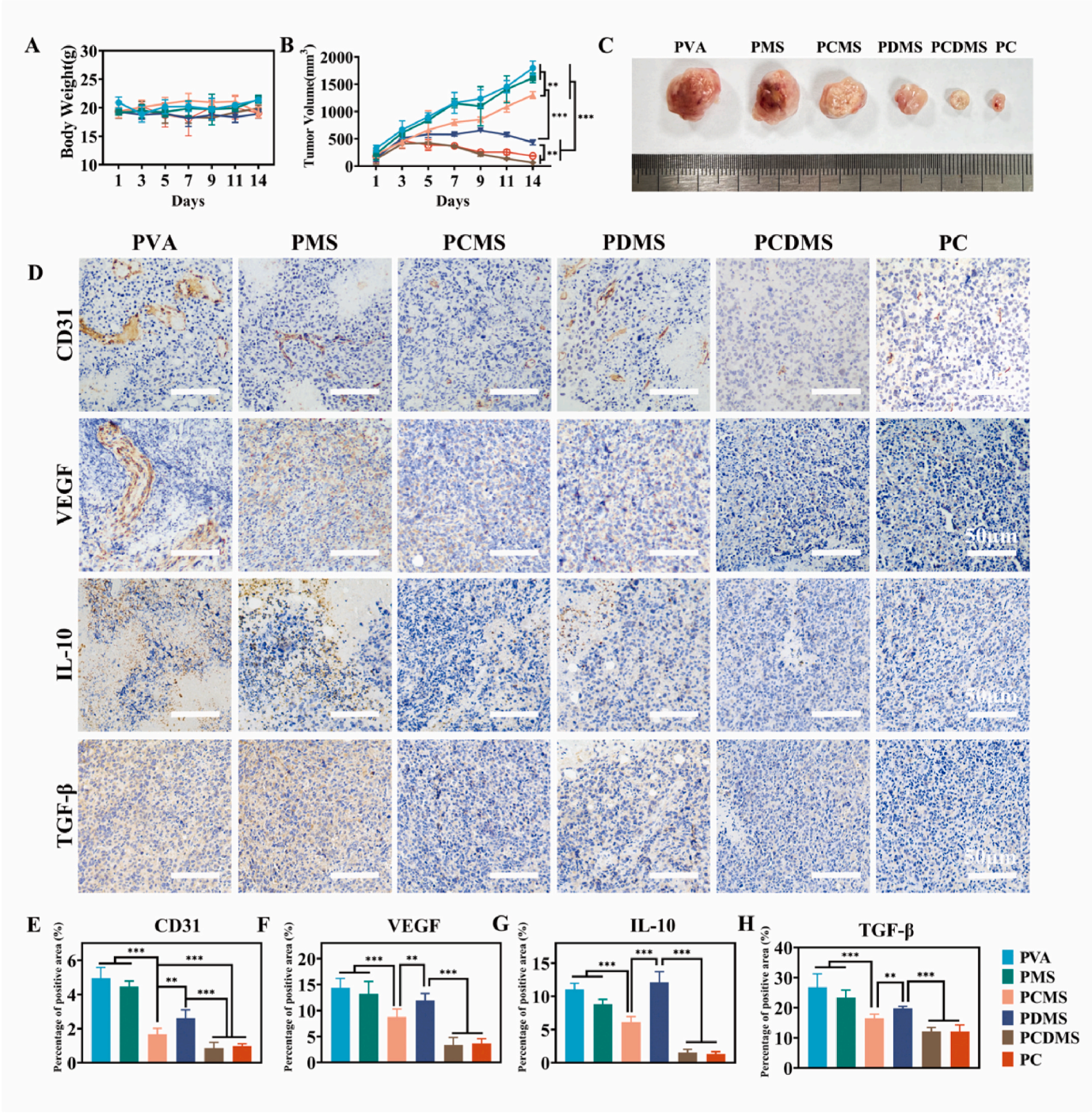

Fig. 4. Suppressive effects of PCDMS on subcutaneous H22 tumor graft in Balb/c mice. **(A)** Changes in body weight of mice in each group after treatment. **(B)** Changes in tumor volume of mice in each group after treatment. **(C)** Representative images of tumors in each group two weeks after treatment. **(D)** Representative immunohistochemical staining images of CD31, VEGF, IL-10, and TGF-β in tumors. Scale bar: 50 μm. **(E-H)** Statistical analysis of the percentage of positive staining area for CD31, VEGF, IL-10, and TGF-β immunohistochemistry. Significant differences: *P < 0.05, **P < 0.01, and ***P < 0.001.

living cells in PCDMS group was close to that in PC group, which was significantly lower than that in other groups.

Furthermore, Annexin V FITC/PI double staining combined with flow cytometry was used to detect cell apoptosis in MHCC-97H and SMMC-7721 cells. The results showed the following in MHCC-97H cells (Fig. 2F,I): the PCMS, PDMS, PCDMS and PC groups exhibited cell cycle arrest, with an increased proportion of cells in the S phase. Particularly, the PCDMS group showed a significant increase in the S phase (72.40 %) and a notable decrease in the G2/M phase (0 %), with significant differences ($p < 0.05$). No significant cell cycle arrest was observed in SMMC-7721 cells (Fig. 3F,I).

3.3. The inhibitory effect of PCDMS on subcutaneous H22 tumor in Balb/c mice

Next, a Balb/c mouse subcutaneous H22 tumor model was established to verify the in vivo therapeutic effect of PCDMS on liver tumors. The body weight and tumor volume were monitored after treatment, and the results showed no significant difference in body weight changes among the groups (Fig. 4A). However, in terms of tumor volume (Fig. 4B–C), mice treated with PDMS and PCDMS exhibited significant tumor shrinkage compared to the PVA, PMS, and PCMS groups, with statistically significant differences. Among them, the tumor volume of PCDMS group was the most significant reduction, similar to that of PC group. On the 15th day after treatment, the mice were euthanized, and tumor tissues were collected for immunohistochemical staining and flow cytometry analysis.

CD31 [19] and VEGF [20] are important markers of liver cancer metastasis and invasion. Immunohistochemical staining results showed abundant expression of CD31 and VEGF in the PVA and PMS groups (Fig. 4D–F). PDMS loaded with DDP also exhibited high expression of CD31 and VEGF. In contrast, PCMS and PCDMS showed inhibition of CD31 and VEGF expression, with the PCDMS group exhibiting the most significant suppression similar to PC group. These results indicate that the combined application of CXB and DDP can significantly inhibit excessive vascular growth in liver cancer.

IL-10 [21] and TGF-β [22] play a dominant role in the tumor microenvironment of various cancers and are mainly responsible for immune suppression. Immunohistochemical staining analysis (Fig. 4D, G, 4H) showed that the expression of IL-10 was higher in PVA, PMS and PDMS groups, while the expression of IL-10 was lower in PCMS and PCDMS groups, among which the expression of PCDMS was the lowest and close to that of PC group. Similar results were observed for the expression of TGF-β. This indicates that the application of CXB to inhibit COX-2 expression can improve the local immune microenvironment of liver cancer and reduce immune suppression.

IL-6 and TNF-α are important indicators related to inflammation [23]. Immunohistochemical results (Supplementary Material Fig. S2A, S2B-C) showed that the proportion of IL-6 and TNF-α positive cells in PCDMS group was the lowest, which was similar to that in PC group, indicating that PCDMS could slow release CXB and DDP to inhibit the occurrence of partial tumor inflammation. The proliferation of the tumor was further evaluated (Supplementary Material Fig. S2A, S2D). The tumor cells in PVA group were dispersed and the proportion of Ki-67 positive cells was the highest. In PCDMS group, the proportion of Ki-67 positive cells was significantly reduced and was close to that in PC group. These results suggest that the PCDMS group can inhibit tumor proliferation.

T cells are important effectors of the immune system against cancer and can be divided into $CD8^+$ T cells and $CD4^+$ T cells [24]. $CD8^+$ T cells are considered to have a direct role in tumor elimination, while $CD4^+$ T cells primarily promote anti-tumor immunity through cytokine secretion and assisting in the activation of $CD8^+$ T cells. In this study, we analyzed the T cell subsets in tumor tissues using flow cytometry and found that the proportion of $CD4^+$ T cells in PVA, PMS, PCMS, PDMS, and PCDMS was 3.26 %, 2.54 %, 12.38 %, 4.73 %, and 12.59 %, respectively, while the proportion of $CD8^+$ T cells in PVA, PMS, PCMS, PDMS, and PCDMS was 0.14 %, 0.55 %, 4.28 %, 2.49 %, and 5.25 %, respectively (Supplementary Material Fig. S3). The results indicate that compared to other groups, PCDMS can significantly promote the infiltration of T cells into the tumor site and enhance the anti-tumor immune response. Histological examination of important organs including the heart, liver, spleen, lungs, and kidneys of mice from each treatment group did not reveal significant pathological changes (Supplementary Material Fig.S4).

3.4. Treatment effect of PCDMS on New Zealand rabbit VX2 hepatic cancer model

Two weeks after the establishment of the VX2 tumor model in the liver of New Zealand rabbits, a contrast-enhanced CT scan was performed for reassessment. The arterial phase of the enhanced CT scan revealed enhanced edges of the VX2 tumor with internal hypodense areas, suggesting internal tumor necrosis and liquefaction (Fig. 5A).

The angiography showed dense vascular distribution around the VX2 tumor in the left lobe of the liver. Following microsphere embolization, the tumor-feeding artery was occluded (Fig. 5B). Enhanced CT scan was performed 1 and 2 weeks after TACE surgery, and large low-density shadows were seen in the embolization region 2 weeks after surgery. The tumor enhancement disappeared, indicating complete tumor necrosis on imaging (Fig. 5C). Gross examination of the liver demonstrated a distinct necrotic area in the left lobe that completely covered the VX2 tumor. On longitudinal sectioning of the tumor, the tumor substance appeared necrotic with ischemic necrosis (Fig. 5D). HE staining showed the presence of embolized microspheres in hepatic vessels and erythrocyte stasis in the embolized local tissue interspaces. In addition, hepatocytes showed cytoplasmic discoloration, vacuole formation, and increased nuclear volume, indicating cell necrosis (Fig. 5E).

To further evaluate the embolization effect of PCDMS on the tumor, PCNA immunofluorescence staining was conducted to assess tumor proliferation. The fluorescence staining results (Fig. 5E) showed a significant decrease in PCNA expression in the PCDMS group compared to the PVA group, with PCMS and PDMS groups also exhibiting decreased PCNA expression, albeit to a lesser extent. These results indicate that PCDMS can effectively inhibit tumor cell proliferation, thereby improving the efficacy of embolization chemotherapy during TACE.

By conducting immunohistochemical staining analysis on tumor tissues, the expression of CTR-1 (a drug influx protein) was found to be higher in the PCDMS group compared to the PDMS group, showing a statistically significant difference ($p < 0.05$) (Fig. 6A–B). MRP-2, an important drug efflux protein, plays a significant role in determining the sustained action of cisplatin within tumor cells [25]. Statistical analysis showed that the expression of MRP-2 in PDMS group was significantly higher than that in PCDMS group, indicating that the combined application of celecoxib inhibiting COX-2 could significantly affect the expression of MRP-2 in HCC cells (Fig. 6A,C). These results indicate that local application of cisplatin can rapidly induce tumor cell resistance (<14 days), while PCDMS, loaded with a significant amount of celecoxib, can slowly release cisplatin at the site of action, upregulate CTR-1 through the inhibition of the COX-2 pathway, and decrease the expression of MRP-2, allowing cisplatin to exert continuous effects within tumor cells and delaying the occurrence of multidrug resistance.

$CD4^+$ T cells and $CD8^+$ T cells are commonly found as immune cytotoxic cells in the tumor microenvironment. Immunofluorescence staining analysis of tumor tissues revealed that the PCDMS group significantly promoted T cell infiltration, especially $CD4^+$ T cells, which play an important role in enhancing anti-tumor immunity (Fig. 6A, E,6F). $Foxp3^+$ T cells are a type of immunosuppressive cell. Evaluation through immunohistochemical staining (Fig. 6A,D) suggested that the PVA, PMS, and PDMS groups exhibited a higher accumulation of regulatory T cells, while the PCMS and PCDMS groups, loaded with celecoxib, showed some differences with weaker immunosuppression,

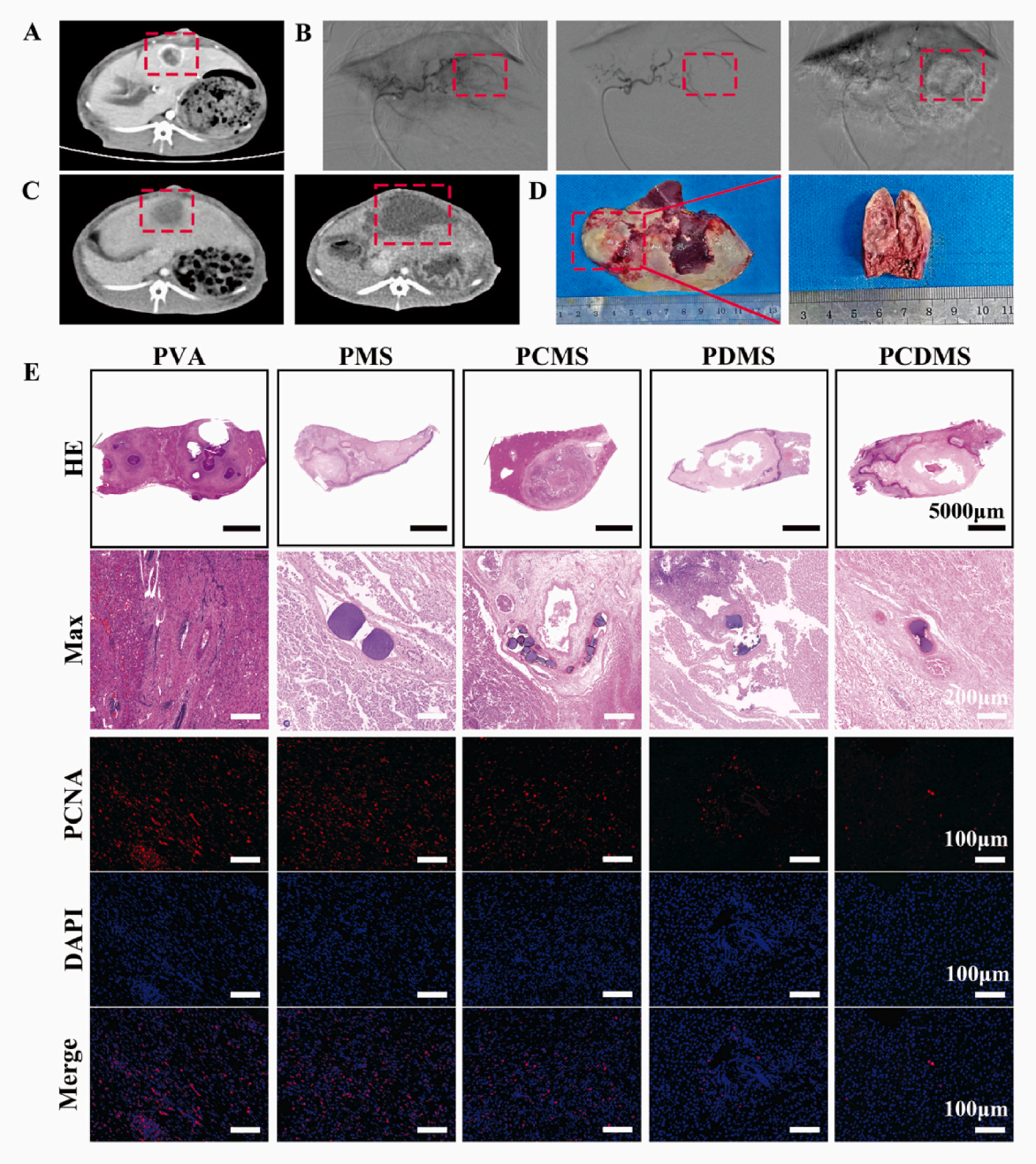

Fig. 5. (A) Enhanced CT scan image two weeks after the construction of the liver VX2 tumor model. **(B)** DSA image during TACE procedure after catheterization of the femoral artery and superselection of the hepatic artery using a 2.7-F microcatheter. **(C)** Enhanced CT scan images taken 1 and 2 weeks after TACE surgery. **(D)** Gross image of the left lobe of the liver 2 weeks after TACE surgery. **(E)** HE staining and PCNA fluorescence staining images of each group after 2 weeks. Scale bar: 100 μm, 200 μm, and 5000 μm.

indicating a more active immune response. The application of celecoxib can regulate the tumor immune microenvironment by inhibiting the expression of COX-2, reducing local inflammatory reactions, and transforming "cold" tumors into "hot" tumors, thereby providing favorable conditions for further immunotherapy.

3.5. Biosafety evaluation

The safety evaluation of celecoxib combined with cisplatin in TACE is an important indicator for its future clinical application. After two weeks of treatment, hematological parameters, liver function, kidney function, and pathological changes of vital organs such as heart, liver, spleen, and kidney were evaluated. The white blood cell count, red blood cell count, and platelet count in all groups remained within the normal range or slightly higher than the theoretical normal values, indicating that cisplatin did not cause significant bone marrow suppression (Fig. 7A–C). In all groups, ALT, AST, ALB, and TBIL levels were significantly elevated within the first week after the procedure (Fig. 7D–G). This elevation was attributed to the short-term ischemic necrosis of tumor tissues and liver cells following TACE, resulting in transient liver function abnormalities. However, by the end of the second week, the levels in all groups had returned to normal (Supplementary material, Tab. 1). Renal function-related indicators, such as Cr and BUN, also exhibited a transient increase (Fig. 7H–I), which returned

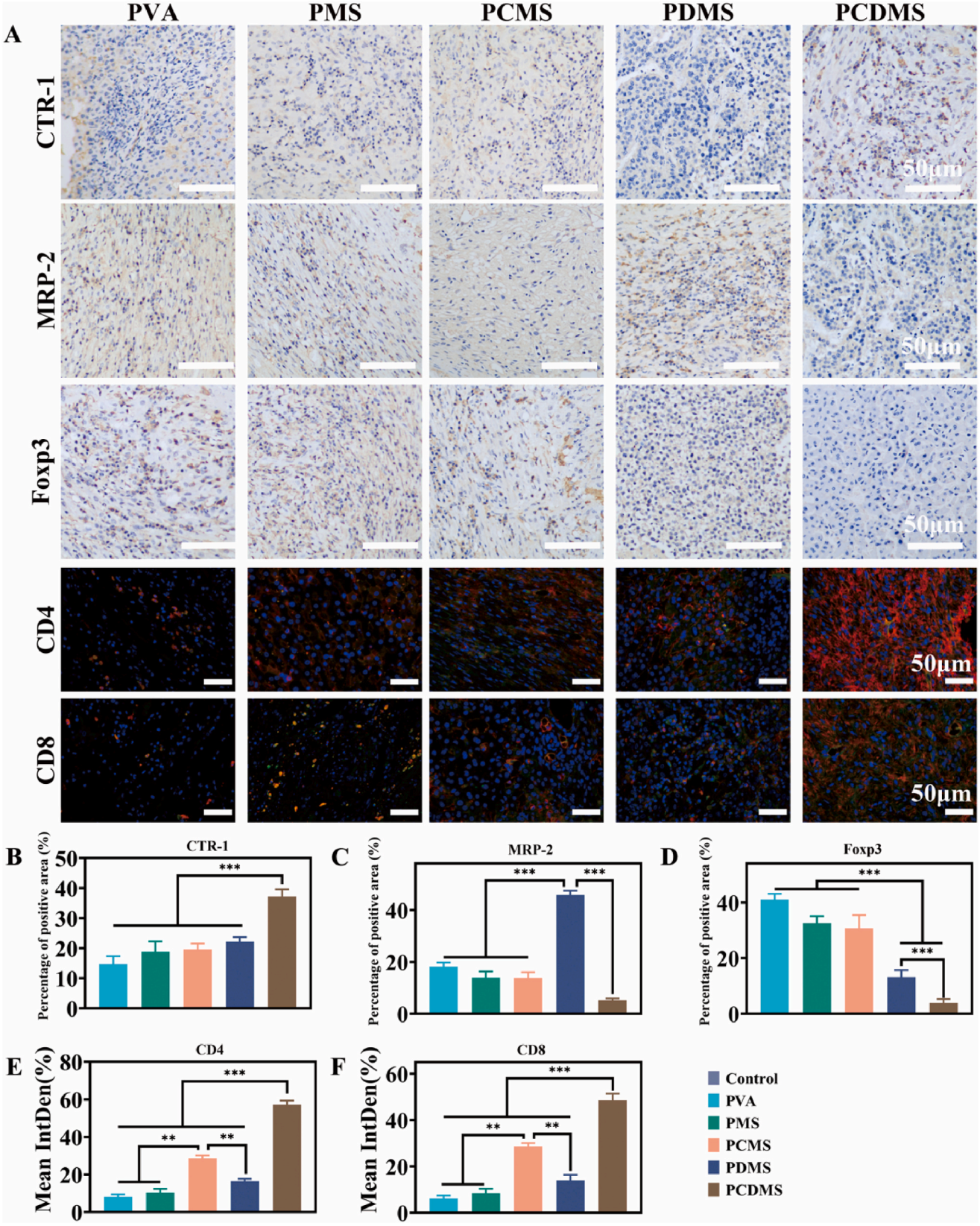

Fig. 6. (A) Immunohistochemical and immunofluorescence staining images of CTR-1, MRP-2, Foxp3, $CD4^+$ T cell, and $CD8^+$ T cell two weeks after TACE for each group. Scale bar: 50 μm. **(B–D)** Statistical analyses of the percentage of positive staining area for CTR-1, MRP-2, and Foxp3 immunohistochemical staining, respectively. **(E–F)** The statistical analyses of the average fluorescence intensity for CD4 and CD8 immunofluorescence staining, respectively. Significant differences: *P < 0.05, **P < 0.01, and ***P < 0.001.

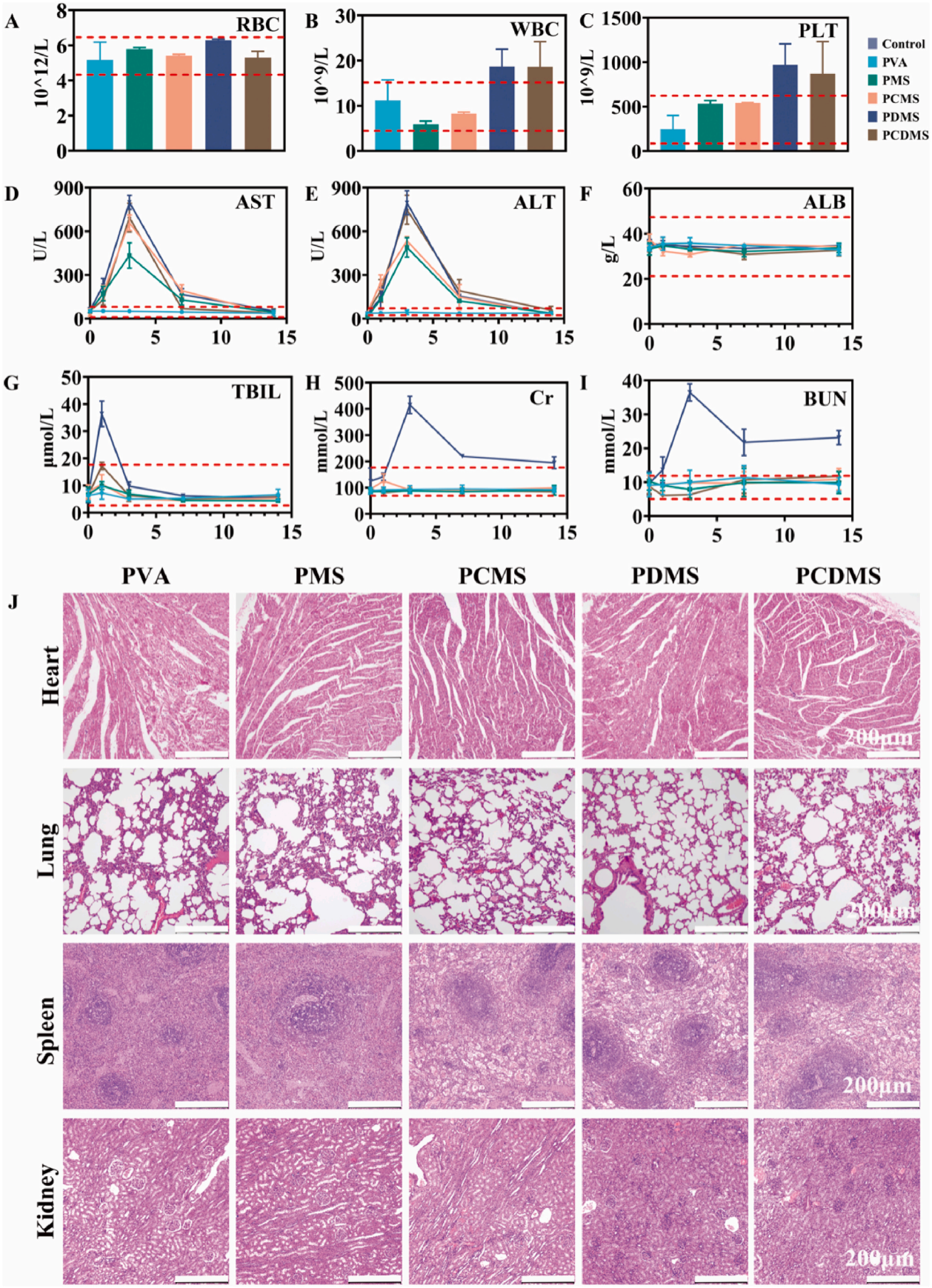

Fig. 7. (A–C) The average values of red blood cells (RBC), white blood cells (WBC), and platelets (PLT) for each group two weeks after TACE. **(D–I)** The changes in liver and kidney function for each group. **(J)** HE staining of the heart, spleen, lung, and kidney for each group two weeks after TACE. Scale bar: 200 μm.

to normal levels after two weeks, except in the PDMS group. Histopathological examination using HE staining revealed no pathological changes in other tissues (Fig. 7J). These results indirectly confirm the relatively high safety profile of the dual-loaded microspheres in TACE for HCC.

4. Discussion

Monotherapy is often insufficient in dealing with advanced cancer due to the multiple mechanisms of disease progression and self-proliferation exhibited by cancer cells. It is difficult for a single anti-cancer drug to completely inhibit the disease process [26]. Therefore, combination therapy, which achieves a synergistic effect where "1 + 1>2," is a crucial approach in anti-tumor research. Cisplatin, as a first-generation platinum-based chemotherapy drug, exhibits a unique mechanism of action primarily by interfering with DNA replication, thereby inhibiting the rapid proliferation of tumor cells and inducing programmed cell death. However, patients undergoing treatment are prone to developing resistance, thereby affecting the therapeutic efficacy. Previous research findings [27] have shown that overexpression of cyclooxygenase-2 (COX-2) is observed in cisplatin-resistant tumor cells. Xu et al. [27] proposed that COX-2 may be involved in P-glycoprotein (P-GP)-mediated drug resistance, and celecoxib enhances the cytotoxic effects of chemotherapy drugs by inhibiting this enzyme. The levels of Ki67 and PCNA, when cisplatin and celecoxib are administered in combination, are significantly superior to those achieved with cisplatin monotherapy. However, in some early clinical trials, combined treatment with celecoxib did not significantly improve patients' progression-free survival [28]. It has been suggested that this may be due to the limited local accumulation caused by systemic administration of celecxib, combined with its short half-life of only 11 h, thus limiting its full potential for anti-tumor effects [29]. The clinical application of transarterial chemoembolization (TACE) and drug-eluting microspheres provides a new approach to the combination therapy of cisplatin and celecoxib. TACE enables the targeted delivery of embolic microspheres loaded with a large number of drugs to the tumor site, ensuring sustained and controlled release, thereby effectively exerting its antitumor effect while reducing systemic side effects and improving patient tolerability.

Additionally, this work demonstrated that PCDMS treatment for VX2 liver transplantation tumors in rabbits is safe and effective. It induces tumor cell apoptosis, inhibits tumor cell proliferation, and slows down the development of cisplatin resistance through the inhibition of the COX-2 pathway. Additionally, it can modulate the local immune microenvironment to stimulate anti-tumor immune responses, thus creating favorable conditions for subsequent immunotherapy.

In summary, this study provides evidence for the use of celecoxib in combination with cisplatin through TACE surgery as a synergistic treatment for liver cancer. Further in-depth research is needed to provide more reasonable and reliable data and theoretical support for clinical applications in the future. However, it is important to acknowledge certain limitations of this study. For instance, the animal model used is relatively limited, and future research could involve constructing various models to investigate the topic more comprehensively. Moreover, this study did not delve into the molecular mechanisms by which celecoxib regulates tumor resistance and immune responses, which could be addressed in future investigations.

5. Conclusion

In conclusion, we successfully prepared dual-loaded microspheres by utilizing polydopamine-modified polyethylene glycol particles. Using the inherent properties of polydopamine, PCDMS showed effective loading and sustained release of celecoxib and cisplatin. Furthermore, the combined application of celecoxib and cisplatin overcame the resistance of liver cancer cells to cisplatin, reshaped the local tumor microenvironment, and effectively suppressed tumor growth and recurrence, achieving a synergistic anti-tumor effect where 1 + 1>2. Overall, PCDMS holds great potential for the treatment of refractory liver cancer and presents significant translational possibilities.

Funding

This work was supported by National Natural Science Foundation of China (82302328, 32000940), Major Science and Technology Special Project of Henan Province (221100310100), Medical Science and Technology Project of Henan Province (LHGJ20200296), Health Commission of Henan Province (SBGJ202103047), 2023 Industry-University-Research-Application Science and Techology Innovation Team Cultivation Project (32214113) and Horizontal Research Program of Zhengzhou University (24110005).

CRediT authorship contribution statement

Kunpeng Wu: Investigation, Methodology, Visualization, Writing - original draft. **Shengnan Ma:** Investigation, Supervision. **Xiaohong Xu:** Methodology, Visualization. **Yiming Liu:** Investigation, Methodology, Visualization. **Chuan Tian:** Visualization. **Chengzhi Zhang:** Investigation. **Jiheng Shan:** Methodology. **Zongming Li:** Visualization. **Kewei Ren:** Investigation. **Jianzhuang Ren:** Supervision. **Xinwei Han:** Conceptualization, Supervision, Writing - review & editing. **Yanan Zhao:** Conceptualization, Supervision, Writing - original draft, Writing - review & editing.

Declaration of competing interest

The authors declare that they have no known competing financial interests or personal relationships that could have appeared to influence the work reported in this paper.

Data availability

Data will be made available on request.

Appendix A. Supplementary data

Supplementary data to this article can be found online at https://doi.org/10.1016/j.mtbio.2023.100927.

References

[1] H. Sung, J. Ferlay, R.L. Siegel, M. Laversanne, I. Soerjomataram, A. Jemal, F. Bray, CA A Cancer J. Clin. 71 (3) (2021) 209, https://doi.org/10.3322/caac.21660.
[2] J.M. Llovet, R.K. Kelley, A. Villanueva, A.G. Singal, E. Pikarsky, S. Roayaie, R. Lencioni, K. Koike, J. Zucman-Rossi, R.S. Finn, Nat. Rev. Dis. Prim. 7 (1) (2021) 6, https://doi.org/10.1038/s41572-020-00240-3.
[3] D. Anwanwan, S.K. Singh, S. Singh, V. Saikam, R. Singh, Biochim. Biophys. Acta Rev. Canc 1873 (1) (2020), 188314, https://doi.org/10.1016/j.bbcan.2019.188314.
[4] Y.S. Liu, M.C. Ou, Y.S. Tsai, X.Z. Lin, C.K. Wang, H.M. Tsai, M.T. Chuang, Korean J. Radiol. 16 (1) (2015) 125, https://doi.org/10.3348/kjr.2015.16.1.125.
[5] a) Y.X. Wáng, T. De Baere, J.M. Idée, S. Ballet, Chin. J. Cancer Res. 27 (2) (2015) 96, https://doi.org/10.3978/j.issn.1000-9604.2015.03.03;
b) G. Zhao, S. Liu, S. Chen, Z. Ren, C. Li, J. Bian, J. Wu, J. Zhou, Y. Zhang, Drug Deliv. 28 (1) (2021) 1356, https://doi.org/10.1080/10717544.2021.1943057.
[6] a) J. Kettenbach, A. Stadler, I.V. Katzler, R. Schernthaner, M. Blum, J. Lammer, T. Rand, Cardiovasc. Intervent. Radiol. 31 (3) (2008) 468, https://doi.org/10.1007/s00270-007-9280-6;
b) M.M. Welling, N. Duszenko, M.P. van Meerbeek, T.J.M. Molenaar, T. Buckle, F. W.B. van Leeuwen, D.D.D. Rietbergen, J. Clin. Med. 12 (3) (2023), https://doi.org/10.3390/jcm12030918.
[7] X. Zheng, J. Zhang, J. Wang, X. Qi, J.M. Rosenholm, K. Cai, J. Phys. Chem. C 119 (43) (2015), 24512, https://doi.org/10.1021/acs.jpcc.5b08558.
[8] Y. Liu, K. Ai, L. Lu, Chem. Rev. 114 (9) (2014) 5057, https://doi.org/10.1021/cr400407a.
[9] a) W. Sieghart, F. Hucke, M. Peck-Radosavljevic, J. Hepatol. 62 (5) (2015) 1187, https://doi.org/10.1016/j.jhep.2015.02.010;
b) A.S. Mikhail, A.H. Negussie, M. Mauda-Havakuk, J.W. Owen, W.F. Pritchard, A.

L. Lewis, B.J. Wood, Expet Opin. Drug Deliv. 18 (3) (2021) 383, https://doi.org/10.1080/17425247.2021.1835858;
c) R. Dutta, R.I. Mahato, Pharmacol. Ther. 173 (2017) 106, https://doi.org/10.1016/j.pharmthera.2017.02.010.
[10] a) S. Ghosh, Bioorg. Chem. 88 (2019), 102925, https://doi.org/10.1016/j.bioorg.2019.102925;
b) S. Dasari, P.B. Tchounwou, Eur. J. Pharmacol. 740 (2014) 364, https://doi.org/10.1016/j.ejphar.2014.07.025.
[11] a) L. Qi, Q. Luo, Y. Zhang, F. Jia, Y. Zhao, F. Wang, Chem. Res. Toxicol. 32 (8) (2019) 1469, https://doi.org/10.1021/acs.chemrestox.9b00204;
b) F. Shahid, Z. Farooqui, F. Khan, Eur. J. Pharmacol. 827 (2018) 49, https://doi.org/10.1016/j.ejphar.2018.03.009.
[12] J.V. Cruz, J.M.C. Rosa, N.M. Kimani, S. Giuliatti, C.B.R. Dos Santos, Curr. Med. Chem. 29 (17) (2022) 3028, https://doi.org/10.2174/0929867328666210910125229.
[13] a) W.Z. Li, Q.J. Huo, X.Y. Wang, F. Xu, Prostag. Other Lipid Mediat. 93 (3–4) (2010) 113, https://doi.org/10.1016/j.prostaglandins.2010.08.001;
b) W.Z. Li, X.Y. Wang, Y.Q. Ding, Nan Fang Yi Ke Da Xue Xue Bao 29 (3) (2009) 466;
c) C.H. Zuo, Z.R. Li, X. Zhou, Y.Z. Ouyang, Z.Y. Zhou, L. Zeng, Ai Zheng 25 (4) (2006) 414.
[14] a) K.R. Roy, G.V. Reddy, L. Maitreyi, S. Agarwal, C. Achari, S. Vali, P. Reddanna, Cancer Chemother. Pharmacol. 65 (5) (2010) 903, https://doi.org/10.1007/s00280-009-1097-3;
b) O. Fantappiè, M. Solazzo, N. Lasagna, F. Platini, L. Tessitore, R. Mazzanti, Cancer Res. 67 (10) (2007) 4915, https://doi.org/10.1158/0008-5472.Can-06-3952.
[15] a) M. Hennequart, L. Pilotte, S. Cane, D. Hoffmann, V. Stroobant, E. Plaen, B. J. Van den Eynde, Cancer Immunol. Res. 5 (8) (2017) 695, https://doi.org/10.1158/2326-6066.Cir-16-0400;
b) S.Y. Lee, H.K. Choi, K.J. Lee, J.Y. Jung, G.Y. Hur, K.H. Jung, J.H. Kim, C. Shin, J.J. Shim, K.H. In, K.H. Kang, S.H. Yoo, J. Immunother. 32 (1) (2009) 22, https://doi.org/10.1097/CJI.0b013e31818ac2f7;
c) Y. Nakanishi, M. Nakatsuji, H. Seno, S. Ishizu, R. Akitake-Kawano, K. Kanda, T. Ueo, H. Komekado, M. Kawada, M. Minami, T. Chiba, Carcinogenesis 32 (9) (2011) 1333, https://doi.org/10.1093/carcin/bgr128;
d) V. Prima, L.N. Kaliberova, S. Kaliberov, D.T. Curiel, S. Kusmartsev, Proc. Natl. Acad. Sci. U.S.A. 114 (5) (2017) 1117, https://doi.org/10.1073/pnas.1612920114.
[16] X. Li, X. Ji, K. Chen, M.W. Ullah, X. Yuan, Z. Lei, J. Cao, J. Xiao, G. Yang, Biomater. Sci. 8 (10) (2020) 2797, https://doi.org/10.1039/c9bm01775e.
[17] Y. Zhao, C. Tian, Y. Liu, Z. Liu, J. Li, Z. Wang, X. Han, Biomaterials 295 (2023), 122029, https://doi.org/10.1016/j.biomaterials.2023.122029.
[18] C. Tian, Z. Wang, L. Huang, Y. Liu, K. Wu, Z. Li, B. Han, D. Jiao, X. Han, Y. Zhao, J. Transl. Med. 20 (1) (2022) 463, https://doi.org/10.1186/s12967-022-03653-8.
[19] Y.Y. Zhang, L.Q. Kong, X.D. Zhu, H. Cai, C.H. Wang, W.K. Shi, M.Q. Cao, X.L. Li, K. S. Li, S.Z. Zhang, Z.T. Chai, J.Y. Ao, B.G. Ye, H.C. Sun, Cancer Lett. 429 (2018) 29, https://doi.org/10.1016/j.canlet.2018.05.004.
[20] J. Lin, S. Cao, Y. Wang, Y. Hu, H. Liu, J. Li, J. Chen, P. Li, J. Liu, Q. Wang, L. Zheng, J. Exp. Clin. Cancer Res. 37 (1) (2018) 113, https://doi.org/10.1186/s13046-018-0727-1.
[21] K.M. Sullivan, X. Jiang, P. Guha, C. Lausted, J.A. Carter, C. Hsu, K.P. Labadie, K. Kohli, H.L. Kenerson, S.K. Daniel, X. Yan, C. Meng, A. Abbasi, M. Chan, Y.D. Seo, J.O. Park, I.N. Crispe, R.S. Yeung, T.S. Kim, T.S. Gujral, Q. Tian, S.C. Katz, V. G. Pillarisetty, Gut 72 (2) (2023) 325, https://doi.org/10.1136/gutjnl-2021-325808.
[22] J. Chen, J.A. Gingold, X. Su, Trends Mol. Med. 25 (11) (2019) 1010, https://doi.org/10.1016/j.molmed.2019.06.007.
[23] a) K. Taniguchi, M. Karin, Semin. Immunol. 26 (1) (2014) 54, https://doi.org/10.1016/j.smim.2014.01.001;
b) D.J. Propper, F.R. Balkwill, Nat. Rev. Clin. Oncol. 19 (4) (2022) 237, https://doi.org/10.1038/s41571-021-00588-9.
[24] D.J. Pinato, S.M. Murray, A. Forner, T. Kaneko, P. Fessas, P. Toniutto, B. Mínguez, V. Cacciato, C. Avellini, A. Diaz, R.J. Boyton, D.M. Altmann, R.D. Goldin, A. U. Akarca, T. Marafioti, F.A. Mauri, E. Casagrande, F. Grillo, E. Giannini, S. Bhoori, V. Mazzaferro, J Immunother Cancer 9 (9) (2021), https://doi.org/10.1136/jitc-2021-003311.
[25] E. Herraez, L. Sanchez-Vicente, R.I.R. Macias, O. Briz, J.J.G. Marin, Oncotarget 8 (21) (2017), 34617, https://doi.org/10.18632/oncotarget.16119.
[26] D. Plana, A.C. Palmer, P.K. Sorger, Cancer Discov. 12 (3) (2022) 606, https://doi.org/10.1158/2159-8290.Cd-21-0212.
[27] H.B. Xu, F.M. Shen, Q.Z. Lv, Eur. J. Pharmacol. 776 (2016) 1, https://doi.org/10.1016/j.ejphar.2016.02.035.
[28] a) D.J. Kerr, S. Chamberlain, R.S. Kerr, JAMA 325 (13) (2021) 1257, https://doi.org/10.1001/jama.2021.2651;
b) J.A. Meyerhardt, Q. Shi, C.S. Fuchs, J. Meyer, D. Niedzwiecki, T. Zemla, P. Kumthekar, K.A. Guthrie, F. Couture, P. Kuebler, J.C. Bendell, P. Kumar, D. Lewis, B. Tan, M. Bertagnolli, A. Grothey, H.S. Hochster, R.M. Goldberg, A. Venook, C. Blanke, E.M. O'Reilly, A.F. Shields, JAMA 325 (13) (2021) 1277, https://doi.org/10.1001/jama.2021.2454;
c) H. Hu, L. Kang, J. Zhang, Z. Wu, H. Wang, M. Huang, P. Lan, X. Wu, C. Wang, W. Cao, J. Hu, Y. Huang, L. Huang, H. Wang, L. Shi, Y. Cai, C. Shen, J. Ling, X. Xie, Y. Cai, X. He, R. Dou, J. Zhou, T. Ma, X. Zhang, S. Luo, W. Deng, L. Ling, H. Liu, Y. Deng, Lancet Gastroenterol Hepatol 7 (1) (2022) 38, https://doi.org/10.1016/s2468-1253(21)00348-4.
[29] A.F. Khafaga, R.N. Shamma, A. Abdeen, A.M. Barakat, A.E. Noreldin, A. O. Elzoghby, M.A. Sallam, Nanomedicine (Lond) 16 (19) (2021) 1691, https://doi.org/10.2217/nnm-2021-0086.